



HAL
open science

Metal–biomolecule frameworks (BioMOFs): a novel approach for “green” optoelectronic applications

Cristina Martin, Dries Jonckheere, Eduardo Coutino-Gonzalez, Simon Smolders, Bart Bueken, Carlos Marquez, Andraž Krajnc, Tom Willhammar, Koen Kennes, Olivier James Fenwick, et al.

► To cite this version:

Cristina Martin, Dries Jonckheere, Eduardo Coutino-Gonzalez, Simon Smolders, Bart Bueken, et al.. Metal–biomolecule frameworks (BioMOFs): a novel approach for “green” optoelectronic applications. *Chemical Communications*, 2021, 58 (5), pp.677-680. 10.1039/D1CC05214D . hal-03683806

HAL Id: hal-03683806

<https://hal.science/hal-03683806>

Submitted on 31 May 2022

HAL is a multi-disciplinary open access archive for the deposit and dissemination of scientific research documents, whether they are published or not. The documents may come from teaching and research institutions in France or abroad, or from public or private research centers.

L'archive ouverte pluridisciplinaire **HAL**, est destinée au dépôt et à la diffusion de documents scientifiques de niveau recherche, publiés ou non, émanant des établissements d'enseignement et de recherche français ou étrangers, des laboratoires publics ou privés.

COMMUNICATION

Metal-Biomolecule Frameworks (BioMOFs): a novel approach for “green” optoelectronic applications

Received 00th January 20xx,
Accepted 00th January 20xx

DOI: 10.1039/x0xx00000x

Cristina Martin,^{a,b,*} Dries Jonckheere,^c Eduardo Coutino-Gonzalez,^d Simon Smolders,^c Bart Bueken,^c Carlos Marquez,^c Andraž Krajnc,^e Tom Willhammar,^f Koen Kennes,^a Oliver Fenwick,^{g,h} Fanny Richard,^h Paolo Samorì,^h Gregor Mali,^e Johan Hofkens,^a Maarten B. J. Roeffaers,^{c,*} Dirk E. De Vos^{c,*}

In this study, a water-stable microcrystalline bioMOF was synthesized, characterized, and loaded with silver ions or highly emissive rare earth (RE) metals like Eu³⁺/Tb³⁺. The obtained materials were used as active layer in a proof-of-concept sustainable light-emitting device, highlighting the potential of bioMOFs in optoelectronic applications.

Since the electronic revolution in 20th century, the extensive use of solid-state electronics along with the shortening device lifecycle generate globally 20-50 million tons of electronic waste (e-waste) per year.¹ Although large efforts are being made to manage and dispose e-waste, the presence of toxic heavy elements or non-biodegradable materials in most of the displays (perovskites, quantum dots, or plastics) is forcing to seek alternative sustainable strategies.² Therefore, the development of novel environmentally friendly materials based on biodegradable and ecologically safe approaches (using low or non-toxic materials) is considered as a suitable solution for designing the next generation of electronic devices, known as “green” electronics.³

Thus far, “green” electronic devices have been developed by using biological materials like natural dyes, proteins, plant cellulose, nucleic acids, or nucleobases, to cite a few.⁴ However, the limitations of biodegradable materials as well as the lack of green processing

methods demand novel approaches to expand the palette of biomaterials and low-cost processing strategies. In this regard, metal-biomolecule frameworks (also known as bioMOFs) could offer a convenient solution to integrate biological species with a molecular level control and uniform nanoscale pores, which could result in versatile host materials with tuneable optoelectronic properties.^{5–9} Hitherto, some metal-organic frameworks (MOFs) have been used in novel energy-efficient light-emitting devices (LEDs)^{10–13}; nevertheless, to the best of our knowledge, this is the first time a bioMOF is proposed as an electroluminescent material for the development of LEDs. Up to now, the large crystal sizes of bioMOFs have hindered their application in LEDs due to aggregation caused quenching (ACQ) severely reducing the emission properties of bioMOFs.¹⁴ This, together with their limited water stability (which normally bleaches the emission) hampers economically feasible applications.¹⁵

To overcome these limitations, a novel synthetic path for a water stable bioMOF (IISERP-MOF27)¹⁶, further referred to as BDC bioMOF, allows an easier, fast, and more environmentally approach for BDC bioMOF (1 day vs. 5 days for IISERP-MOF27, further details in ESI), resulting in microcrystalline ‘desert rose’ like crystal aggregates with nanometre thickness crystallites (Figure 1 and S2).

^a KU Leuven, Leuven Chem&Tech - Molecular Imaging and Photonics (MIP), Celestijnenlaan 200F post box 2404, 3001 Leuven, Belgium

^b Unidad nanoCRIB. Centro Regional de Investigaciones Biomédicas, 02071, Albacete, Spain

^c KU Leuven, Leuven Chem&Tech - Centre for Membrane Separations, Adsorption, Catalysis and Spectroscopy for Sustainable Solutions (cMACS), Celestijnenlaan 200F post box 2454, 3001 Leuven, Belgium

^d Centro de Investigaciones en Óptica, A. C. Loma del Bosque 115, Colonia Lomas del Campestre, León, Guanajuato 37150, Mexico

^e Department of Inorganic Chemistry and Technology, National Institute of Chemistry, Hajdrihova 19, 1001 Ljubljana, Slovenia

^f Department of Materials and Environmental Chemistry, Stockholm University, Svante Arrhenius väg 16C, 106 91 Stockholm, Sweden

^g Queen Mary University of London, School of Engineering and Materials Science, Mile End Road, London E1 4NS, United Kingdom

^h University of Strasbourg, CNRS, ISIS UMR 7006, 8 Allée Gaspard Monge, Strasbourg 67000, France

Electronic supplementary information (ESI) available. See DOI:

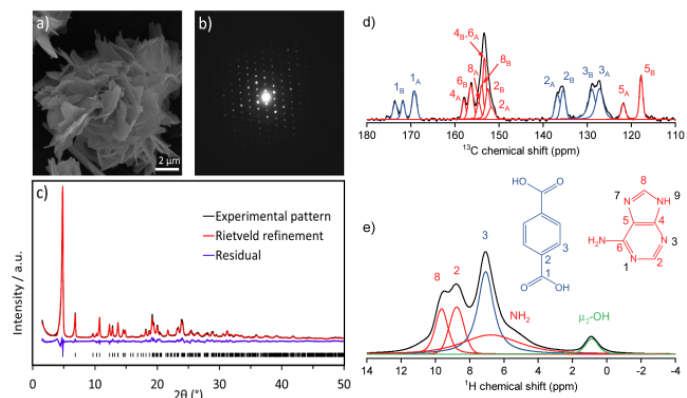


Figure 1. SEM micrograph of BDC bioMOF displaying the desert rose morphology (a). Diffraction pattern of BDC bioMOF obtained from

cRED (b) and Rietveld plot of BDC bioMOF (c). Vertical bars mark the allowed reflections. Deconvoluted (d) ^{13}C and (e) ^1H MAS NMR spectra of BDC bioMOF showing the presence of two distinct BDC and Ad linkers, and of bridging hydroxyls $\mu_2\text{-OH}$.

The smaller crystal size is of paramount importance in electroluminescent applications because large particles can suffer from ACQ, thereby reducing the luminescence efficiency of the material.

The crystal structure of BDC bioMOF was determined using 3D electron diffraction data and the continuous rotation electron diffraction (cRED) technique in the monoclinic space group $C2/c$, refined using SHELXL¹⁷ and confirmed by Rietveld refinement of powder X-ray diffraction (PXRD) data (Figure 1, further details in ESI, Figures S3-S6).

BDC bioMOF consists of infinite two-dimensional layers, pillared by rows of terephthalate linkers (BDC_B), ultimately yielding one-dimensional channels along the [001] direction of approximately 10 Å in diameter (Figure S3). The layers feature a complex architecture involving two distinct Zn^{2+} dimers ($\text{Zn}_1\text{-Zn}_1$ and $\text{Zn}_2\text{-}\mu_2\text{O-Zn}_2$), two distinct adeninate linkers (1:2 ratio $\text{Ad}_A\text{:Ad}_B$) and one terephthalate linker (BDC_A). The chemical composition, $[\text{Zn}_4\text{O}(\text{Ad})_3(\text{BDC})_2]^{1-}$, of BDC bioMOF derived from diffraction experiments reveals an excess of negative charges in the framework, indicating a lack of lightweight cations such as protons. Therefore, solid-state MAS NMR experiments were conducted to study the presence of species/atoms that cannot be detected via diffraction techniques. First, all linker ^1H and ^{13}C NMR signals were identified, which nicely agreed with the presence of two chemically different terephthalate and adeninate linkers in a 1:1 $\text{BDC}_A\text{:BDC}_B$ and a 1:2 $\text{Ad}_A\text{:Ad}_B$ ratio (Figure 1d, details in ESI, Figures S4-S9). Importantly, no other organic species were observed, which indicates that the protons with the signal at approximately 1 ppm (Figure 1e) in the ^1H NMR spectrum are directly attached to the framework. The signal can be ascribed to a $\mu_2\text{-OH}$ in the $\text{Zn}_2\text{-}\mu_2\text{OH-Zn}_2$ dimer and the signal intensity indicates full protonation of the Zn_2 dimer.

Benefiting from the uncoordinated -NH_2 and pyrimidine nitrogen atoms on the Ad_B linkers, several cations like Eu^{3+} , Tb^{3+} and Ag^+ were incorporated (see experimental details in the SI for more info). The success of the approach was confirmed by the different emission colours obtained for Eu@BDC bioMOF (red), Tb@BDC bioMOF (green) and Ag@BDC bioMOF (cyan) under UV irradiation (366 nm) (Figure S10). Elemental analysis revealed a guest loading of 0.3, 0.3 and 4.2 wt%, for Eu^{3+} , Tb^{3+} and Ag^+ , respectively. The PXRD patterns of the different guest@BDC bioMOFs (Figure S11-S12) demonstrated that there is no structural rearrangement of the MOF upon metal loading and no metal nanoparticles were observed. Interestingly, also prolonged exposure to water did not alter the bioMOF's structure (Figure S11-S12), which confirms the highly desired water stability. Moreover, the presence of luminescent silver species in the Ag^+ -loaded MOF was confirmed by X-ray photoelectron spectroscopy (XPS), as observed by the peak at 349 eV (Figure S13), and the lack of metallic signatures in the XPS spectra.^{18,19}

Steady-state diffuse reflectance spectroscopy (DRS) shows two main absorption peaks at 220 and 260 nm for the pristine BDC bioMOF, which can be attributed to the electronic transition of $\pi \rightarrow \pi^*$ of the

adeninate linker²⁰ (Figure S14). In addition, small shoulders at 240 and 290 nm probably originate from the BDC linker²⁰.

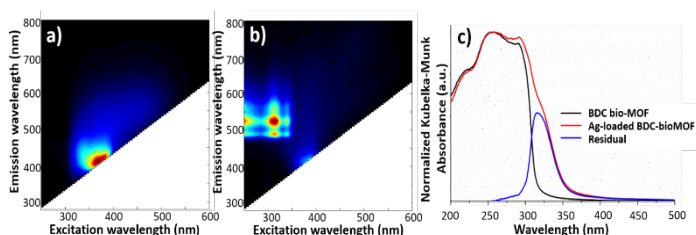


Figure 2. Luminescence excitation-emission maps for (a) pristine BDC bioMOFs and (b) after silver loading. (c) DRS spectra showing a new absorption feature at around 314 nm.

The Kubelka-Munk absorbance spectra of RE loaded MOFs resemble the one of the non-doped BDC bioMOF because the direct excitation of RE metals is parity-forbidden.²¹ However, the steady state UV-Vis spectrum of Ag@BDC bioMOF reveals a new absorption band centred at 314 nm (Figure 2), which was determined by subtracting the parent BDC bioMOF's spectrum from that of the Ag^+ -loaded one. This new band confirms the strong interaction between silver ions and adeninate, as previously observed for other silver-nucleobase metallomacrocyclic interactions.²²

The emission spectrum of the pristine BDC bioMOF can be largely attributed to the photoluminescence of adenine (Figure S15) as the main emission peaks match those observed for the adenine molecule in the solid state. This behaviour was previously observed for bioMOF-1, where the UV absorption and photoluminescence were caused by the adenine molecule, as the 4,4'-biphenyldicarboxylate linker was presumably quenched after incorporation in the bioMOF-1 structure.²³ The Eu^{3+} or Tb^{3+} -loaded BDC bioMOFs displayed completely different emission spectra, as the framework serves as an antenna and transfers excitation energy from the linkers to the RE centres.²³ Figures S16 and S17 show the typical sharp d-f luminescent transitions of lanthanide cations loaded onto BDC bioMOF, viz. Eu^{3+} ($\lambda_{\text{em}} = 657, 615, 652, 700 \text{ nm}$) and Tb^{3+} ($\lambda_{\text{em}} = 490, 545, 585, 625 \text{ nm}$). The absence of the 420 nm band characteristic for bioMOF emission indicates that the energy is effectively transferred from the bioMOF to the RE, as previously observed for other RE doped MOFs.^{22,24,25} On the other hand, the strong interaction between Ag^+ and adenine in silver loaded BDC bioMOF is also visible in its photoluminescent spectra, where the weak emission around 420 nm disappears in favour of a triple-band luminescent feature at $\lambda_{\text{em}} = 490, 525$ and 560 nm (Figure 2b).

To get more insights about the origin of this new emission species, the photoluminescence of Ag^+ -loaded bioMOF was also recorded at 77 K and compared to the standard measurement at room temperature (Figure S18). The low temperature is known to help to determine whether the origin of this new emission species is related to the room temperature phosphorescence (RTP) caused by the strong interaction between polynuclear d^{10} as it was previously described by metal systems with the linker.²⁶ Similar excitation-emission maps were obtained at both temperatures, and they are spectrally analogous to the phosphorescence of aromatic carboxylates.^{27,28} These observations suggest the presence of silver-mediated terephthalate phosphorescence at room temperature. Although room-temperature phosphorescence of such organic

molecules is very rare, it has been recently demonstrated that crystallization-induced phosphorescence in MOFs can be caused by the presence of guests.^{28,29}

To further explore the applicability of BDC-bioMOF, a proof-of-concept bottom-up OLED (organic LED) was constructed with the BDC bioMOF as emissive layer. The MOF was first mixed with a polymer matrix to produce a cost-effective, processable and high-quality film. Purely inorganic electroluminescent materials are known to form inhomogeneous films, thereby reducing carrier injection/mobility and thus overall efficiency.^{30,31} Although semiconducting polymers like polyvinyl carbazole (PVK) can help enhancing the charge mobility in the device,³² polystyrene (PS) was chosen because its absence of charge carrier injection/transport mechanism^{33–35}. By doing that, the results can be ascribed to the OLED's electroluminescence to the BDC bioMOF. PS cannot alter the electronic properties of the MOF, but it has previously been reported that PS could modify the photoluminescence behaviour of the composites due to specific and non-specific interactions.³⁶ Nevertheless, this is not case in this study because the luminescent spectra of the BDC bioMOF do not differ from its PS composite, demonstrating the absence of alterations by the organic matrix (Figure S19). So far, the design of the OLED has been based on the emissive layer, nevertheless, knowing that the quantum yield for all the MOFs are around 5%, a good optimization of charge carrier injection and mobility would be critical to get a high-quality device performance.³⁶ Therefore, each component in the device should be adapted to the electronic structure of the bioMOF. Photoelectron spectroscopy in air (PESA) suggests that ITO (-4.8 eV) and aluminium (-4.3 eV) electrodes are the best candidates to obtain an appropriate charge injection and carrier mobility. Based on this information, an 8 mm² device consisting of vertically stacked: ITO anode / PEDOT:PSS (40 nm) / MOF (300 nm) / Al cathode (150 nm) was built. Figure 3 displays a scheme of the OLED and a typical current-voltage curve of non-doped and doped materials.

Among all the obtained data, the best optoelectronic properties were observed for the OLEDs based on Ag@BDC bioMOF, where the turn-on voltage is decreased (from 11 V in case of the non-doped BDC bioMOF to 6 V) while the EL intensity increases 2.5-fold compared to the pristine BDC bioMOF. This enhancement could originate from: a) the improved carrier mobility by the presence of Ag⁺ cations in the pores which generate an alternative pathway to transport the electrons and holes, and b) the RTP mechanism which hinders the non-radiative triplet emission. Both mechanisms have been previously observed in related OLED configurations,^{33,37,38} and in this case both processes are expected to contribute in boosting the OLED's efficiency. The Eu³⁺ or Tb³⁺-loaded BDC bioMOFs cannot rely on these mechanisms and consequently feature worse performances in terms of carrier mobility (higher turn-on voltages) and brightness (lower EL intensity). It is worth to note that all experiments were conducted outside of the glove box for non-sealed devices, which confirmed the OLED's stability toward water and oxygen.

Even though Ag@BDC bioMOF LED displays the best performance, the same EL spectra were observed for all guest@BDC bioMOFs and the pristine BDC bioMOF (Figure 3), indicating the same origin of the electroluminescent emission.

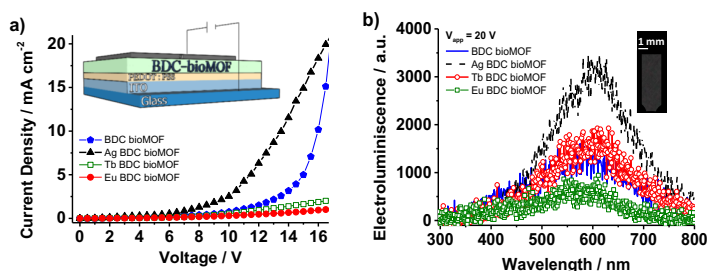


Figure 3. Current density voltage (a) and electroluminescence spectra (b) of non-doped and doped OLEDs. The inset in a) is a schematic representation of the OLED configuration. The inset in b) displays a picture of the device under 20 V.

To unravel this origin, the electroluminescence (EL) spectra of non-loaded BDC bioMOF were recorded at various voltages (Figure S20). While no change in the shape or in the full width at half maximum was observed at higher driving voltages (30 V, bias where breakdown occurs), the intensity maximum (at ~ 600 nm) increased by about a factor of thirty. Remarkably, the maximum of the EL band is bathochromically (red-shifted) by ~ 12745 cm⁻¹ in comparison to the photoluminescence (PL) emission spectrum displayed in Figure S15-S19. The large mismatch between the PL and EL spectra suggests that different excited state species are generated under forward voltage compared to under UV-light irradiation. A plausible explanation for this different behaviour in the electroluminescence studies is that charge carriers could recombine at the Zn-carboxylate or Zn-μ₂OH nodes of the Zn₂ dimers, at the grain boundaries or at the different defects present in the MOFs,^{10,39–41} as previously reported in related studies on silver-exchanged electroluminescent zeolites^{34,35} or dye-doped Zr-MOFs.³³ A wide range of studies on ZnO nanostructures,⁴² have suggested that the EL of ZnO nanostructures originates from different types of defects; in this case this hypothesis seems very plausible. In these studies, it was proven that the type of defect in ZnO strongly affects the EL maxima;²⁰ for example, orange emission (± 620–690 nm) is attributed to oxygen interstitials, red emission (± 690 - 750 nm) corresponds to oxygen vacancies, while blue electroluminescence (± 400 - 460 nm) could be related to the presence of Zn interstitial defects. Based on these reported values, we assume that the EL behaviour observed in the BDC bioMOF is most likely linked to the presence of oxygen vacancies in the framework, presumably at the Zn₂-μ₂OH-Zn₂ dimers or Zn-carboxylate bonds, as the emission maximum band spans between 500 and 720 nm.

In conclusion, the results show the important role played by defects in the electron-hole recombination and electroluminescence emission of BDC bioMOF-LEDs. However, the possibility of having RTP (by confining silver atoms in the MOF pores) induces a positive effect on the optoelectronic properties of the BDC bioMOF due to the enhancement of charge injection and mobility. The results reveal the large potential of bioMOFs based on RTP to provide a novel and sustainable solution for developing “green” optoelectronic devices. Research funding is acknowledged from the EU-FP7 SACS project (Self-Assembly in Confined Space) (FP7/2007-2013) under grant agreement no. 310651. D.E.D.V acknowledges the Research Foundation Flanders (FWO Vlaanderen) (project G.0256.14N) for support in the frame of research projects, the Flemish government (Methusalem CASAS2). Further, we are grateful to the Research

Foundation Flanders (FWO Vlaanderen) (C.M. and B.B.; grant 12J1716N and 12R1217N, respectively) for individual post-doctoral fellowships. T.W. acknowledges the Swedish Research Council (VR, 2019-05465). A.K. and G.M. acknowledge the financial support from the Slovenian Research Agency (research core funding No. P1-0021). E.C.-G. acknowledges the support from UC-MEXUS funds (grant CN-19-165). P.S. acknowledges the financial support from the Agence Nationale de la Recherche through the Labex project CSC (ANR-10-LABX-0026 CSC) within the Investissement d'Avenir program (ANR-10-120 IDEX-0002-02), the International Center for Frontier Research in Chemistry (icFRC) and the Institut Universitaire de France (IUF).

Conflicts of interest

There are no conflicts to declare.

Notes and references

- World Economic Forum, *World Econ. Forum*, 2019, 1–24.
- W. Li, Q. Liu, Y. Zhang, C. Li, Z. He, W. C. H. Choy, P. J. Low, P. Sonar and A. K. K. Kyaw, *Adv. Mater.*, 2020, 32, 2001591.
- M. Irimia-Vladu, *Chem. Soc. Rev.*, 2014, 43, 588–610.
- K. T. Huang, C. C. Chueh and W. C. Chen, *Mater. Today Sustain.*, 2020, 100057.
- J. An, O. K. Farha, J. T. Hupp, E. Pohl, J. I. Yeh and N. L. Rosi, *Nat. Commun.* 2012 31, 2012, 3, 1–6.
- D. K. Yoo, I. Ahmed, M. Sarker, H. J. Lee, A. Vinu and S. H. Jhung, *Mater. Today*, DOI:10.1016/J.MATTOD.2021.07.021.
- S. Rojas, T. Devic and P. Horcajada, *J. Mater. Chem. B*, 2017, 5, 2560–2573.
- J. An, S. J. Geib and N. L. Rosi, *J. Am. Chem. Soc.*, 2009, 131, 8376–8377.
- H. Cai, Y. L. Huang and D. Li, *Coord. Chem. Rev.*, 2019, 378, 207–221.
- M. R. di Nunzio, E. Caballero-Mancebo, B. Cohen and A. Douhal, *J. Photochem. Photobiol. C Photochem. Rev.*, 2020, 44, 100355.
- H. Kaur, S. Sundriyal, V. Pachauri, S. Ingebrandt, K. H. Kim, A. L. Sharma and A. Deep, *Coord. Chem. Rev.*, 2019, 401, 213077.
- M. Gutiérrez, C. Martín, B. E. Souza, M. Van der Auweraer, J. Hofkens and J. C. Tan, *Appl. Mater. Today*, 2020, 21, 100817.
- M. Gutiérrez, C. Martín, M. Van der Auweraer, J. Hofkens and J. Tan, *Adv. Opt. Mater.*, 2020, 8, 2000670.
- Y. Hong, J. W. Y. Lam and B. Z. Tang, *Chem. Soc. Rev.*, 2011, 40, 5361–5388.
- M. Schaer, F. Nüesch, D. Berner, W. Leo and L. Zuppiroli, *Adv. Funct. Mater.*, 2001, 11, 116–121.
- R. Maity, H. D. Singh, A. K. Yadav, D. Chakraborty and R. Vaidhyanathan, *Chem. – An Asian J.*, 2019, 14, 3736–3741.
- G. M. Sheldrick, *Acta Crystallogr. Sect. C Struct. Chem.*, 2015, 71, 3–8.
- O. Fenwick, E. Coutiño-Gonzalez, F. Richard, S. Bonacchi, W. Baekelant, D. Vos, M. B. J. Roeflaers, J. Hofkens and P. Samorì, *Small*, 2020, 16, 2002063.
- O. Fenwick, E. Coutiño-Gonzalez, D. Grandjean, W. Baekelant, F. Richard, S. Bonacchi, D. De Vos, P. Lievens, M. Roeflaers, J. Hofkens and P. Samorì, *Nat. Mater.*, 2016, 15, 1017–1022.
- N. H. Alvi, K. ul Hasan, O. Nur and M. Willander, *Nanoscale Res. Lett.*, 2011, 6, 130.
- K. Binnemans, *Chem. Rev.*, 2009, 109, 4283–4374.
- C. S. Purohit and S. Verma, *J. Am. Chem. Soc.*, 2006, 128, 400–401.
- J. An, C. M. Shade, D. A. Chengelis-Czegán, S. Petoud and N. L. Rosi, *J. Am. Chem. Soc.*, 2011, 133, 1220–1223.
- S. A. Younis, N. Bhardwaj, S. K. Bhardwaj, K. H. Kim and A. Deep, *Coord. Chem. Rev.*, 2021, 429, 213620.
- S. E. Crawford, X. Y. Gan, P. C. K. Lemaire, J. E. Millstone, J. P. Baltrus and P. R. Ohodnicki, *ACS Sensors*, 2019, 4, 1986–1991.
- X. Chen, Z. He, F. Kausar, G. Chen, Y. Zhang and W. Z. Yuan, *Macromolecules*, 2018, 51, 9035–9042.
- D. Levy and D. Avnir, *J. Photochem. Photobiol. A Chem.*, 1991, 57, 41–63.
- W. Zhao, Z. He and B. Z. Tang, *Nat. Rev. Mater.*, 2020, 5, 869–885.
- H.-R. Wang, X.-G. Yang, J.-H. Qin and L.-F. Ma, *Inorg. Chem. Front.*, 2021, 8, 1942.
- C. Sanchez, P. Belleville, M. Popall and L. Nicole, *Chem. Soc. Rev.*, 2011, 40, 696–753.
- T. P. Nguyen, *Surf. Coatings Technol.*, 2011, 206, 742–752.
- D. Braun, *Mater. Today*, 2002, 5, 32–39.
- M. Gutiérrez, C. Martín, K. Kennes, J. Hofkens, M. Van der Auweraer, F. Sánchez and A. Douhal, *Adv. Opt. Mater.*, 2018, 6, 1701060.
- K. Kennes, C. Martín, W. Baekelant, E. Coutino-Gonzalez, E. Fron, M. B. J. Roeflaers, J. Hofkens and M. Van Der Auweraer, *ACS Appl. Mater. Interfaces*, 2019, 11, 12179–12183.
- K. Kennes, E. Coutino-Gonzalez, C. Martín, W. Baekelant, M. B. J. Roeflaers and M. Van der Auweraer, *Adv. Funct. Mater.*, 2017, 27, 1606411.
- J. Lalevée and J. P. Fouassier, *Dyes and Chromophores in Polymer Science*, John Wiley & Sons, Inc., Hoboken, NJ, USA, 2015.
- A. Khetubol, A. Hassinen, Y. Firdaus, W. Vanderlinden, S. Van Snick, S. Flamée, B. Li, S. De Feyter, Z. Hens, W. Dehaen and M. Van Der Auweraer, *J. Appl. Phys.*, 2013, 114, 173704.
- M. Van der Auweraer, F. C. De Schryver and P. Borsenberger, *Chem. Phys.*, 1994, 186, 409–433.
- A. K. Cheetham, T. D. Bennett, F. X. Coudert and A. L. Goodwin, *Dalt. Trans.*, 2016, 45, 4113–4126.
- Z. Fang, B. Bueken, D. E. De Vos and R. A. Fischer, *Angew. Chemie Int. Ed.*, 2015, 54, 7234–7254.
- W. Xiang, Y. Zhang, Y. Chen, C. J. Liu and X. Tu, *J. Mater. Chem. A*, 2020, 8, 21526–21546.
- A. B. Djuriić, A. M. C. Ng and X. Y. Chen, *Prog. Quantum Electron.*, 2010, 34, 191–259.